Improving Paleoseismic Earthquake Magnitude Estimates with Rupture Length Information: Application to the Puget Lowland, Washington State, U.S.A.

Richard H. Styron*[1,2] and Brian Sherrod[3]

ABSTRACT

Both earthquake displacement and rupture length correlate with magnitude, and, therefore, observations of each from past earthquakes can be used to estimate the magnitude of those earthquakes in the absence of instrumental records. We extend the Bayesian inversion method of Biasi and Weldon (2006), which estimates paleoearthquake magnitude from displacement observations, to incorporate both rupture length and surface displacement measurements into the magnitude inversion. We then use this method on 27 late-Pleistocene to Holocene paleoearthquakes in the Puget Lowland region of Washington. Observations of (typically vertical) fault separation per event range from 0.6 to 7 m, implying net displacement per event of up to 10 ± 4 m for the largest event. Rupture lengths are estimated to vary between the smallest contiguous mapped scarps to the full extent of the faults mapped from geology and geophysical observations. Although, a few of the ruptures may be longer than 150 km, the ruptures have a median of 53 km, indicating that earthquakes in the Puget Lowland have relatively high displacement-to-length ratios. By considering both datasets, we find that all events were between M 6.3 and 7.5, generally consistent with the expected seismicity from the U.S. Geological Survey National Seismic Hazard Map for the region. The simultaneous use of both length and displacement data in the magnitude inversion decreases both the estimated earthquake magnitudes and the uncertainty. The magnitude reduction, in particular, is due to the relatively short rupture lengths possible for Puget Lowland faults. This implies a decrease in the seismic hazard (relative to a displacement-only assessment) to a highly populated and rapidly urbanizing region.

KEY POINTS

- Methods are developed to estimate magnitude of paleoearthquake from both rupture length and displacement.
- Magnitudes of 27 paleoearthquakes from the Puget Lowland region, Washington, U.S.A., are estimated.
- All events are between **M** 6.3 and 7.5, generally lower than displacement-only estimates.

Supplemental Material

INTRODUCTION

A primary objective of paleoseismology is the estimation of the magnitude of earthquakes inferred from the geologic record. These paleoearthquakes are typically described in a shallow trench excavated across a fault scarp or from places where past earthquakes deformed shorelines or other strain markers, in which the data constraining the offset and age of any inferred earthquakes are taken. The magnitude of each event is then determined by scaling offset measurements from the trench with empirical displacement–magnitude relations, such as those by Wells and Coppersmith (1994).

These paleoseismic data and interpretations are vital for a wide range of purposes, from constraining the physics and statistics of earthquake rupture processes (e.g., Rockwell and Ben-Zion, 2007) to characterize fault sources in probabilistic seismic hazard analysis (e.g., Field *et al.*, 2014).

1. Earth Analysis, Portland, Oregon, U.S.A.; 2. Global Earthquake Model Foundation, Via Ferrata, Pavia, Italy; 3. U.S. Geological Survey, Earthquake Science Center, Seattle, Washington, U.S.A.

*Corresponding author: richard.h.styron@gmail.com

Cite this article as Styron, R. H., and B. Sherrod (2020). Improving Paleoseismic Earthquake Magnitude Estimates with Rupture Length Information: Application to the Puget Lowland, Washington State, U.S.A., *Bull. Seismol. Soc. Am.* **XX**, 1–15, doi: 10.1785/0120200193

In the western United States, most faults with evidence of Quaternary activity are poorly characterized, negatively impacting our understanding of deformation patterns and concomitant hazard. An array of such faults cut the Puget Lowland region of western Washington State. Although, decades of paleoseismological research have yielded good understanding of the temporal occurrence of earthquakes on these faults (e.g., Nelson *et al.*, 2014; Sherrod and Gomberg, 2014), the magnitudes of the paleoearthquakes are not yet known well enough to accurately inform the hazard models. Therefore, the U.S. National Seismic Hazard Map (NSHM) uses a combination of an area seismic source in which earthquakes may occur uniformly randomly in space, a source with earthquake locations based on spatially smoothed seismicity, and a few discrete fault sources representing some of the more well-studied faults in the region; these latter fault sources have maximum and characteristic earthquake magnitudes, based on the length of the bedrock fault trace and well-established scaling relationships (Frankel *et al.*, 2002, 2015; Petersen *et al.*, 2008), without consideration of the paleoseismic data that may provide information into the magnitudes of earthquake produced by any given fault.

To be sure, considerable uncertainty exists in the process of estimating the magnitudes of paleoearthquakes. In addition to scatter in the data used to create the displacement–magnitude scaling relations, the observed offset in or near the trench has its own measurement uncertainty and is likely not representative of the mean offset along the paleorupture, simply due to the natural along-strike variability of earthquake ruptures (Hemphill-Haley and Weldon, 1999). This last problem is particularly challenging, as it is both hard to accurately address statistically and can lead to variation in the estimated magnitude of 1–2 magnitude orders (i.e., M 6–8). Building on the work of Hemphill-Haley and Weldon (1999), Biasi and Weldon (2006) devised an effective solution with a Bayesian method that uses a likelihood function derived from empirical slip distribution data to reduce the uncertainty in the posterior magnitude, given a point measurement of displacement.

Surface-rupture length is better correlated with earthquake magnitude than mean displacement (Wells and Coppersmith, 1994), and can, therefore, be used as a similar predictor of paleoearthquake magnitude. In fact, independent measurements of both surface rupture length and displacement can be used to estimate paleoearthquake magnitude more accurately and precisely. In this article, we provide an implementation as an extension of Biasi and Weldon (2006) paleomagnitude inversion. We then apply the technique to a compilation of 27 earthquakes from the Puget Lowland, Washington State, U.S.A. The use of rupture length in the paleoearthquake magnitude inversions is here shown to reduce both the estimated magnitude and the associated uncertainty by a large margin relative to displacement-only estimates of paleoearthquake magnitude. This reduction is related to a regional tendency for these earthquakes to have relatively high-slip magnitudes and relatively short rupture lengths. The converse is that the estimated magnitudes are, in most cases, slightly greater than they would be by solely considering fault length, as the NSHM does for this region. Although, the results here do have implications for seismic hazard analysis in the region, which often uses geologic fault dimensions for fault source characterization, we direct the article more toward paleoseismology, due to the latter field's focus on the magnitudes of individual paleoearthquakes and the use of displacement measurements to constrain them.

PALEOEARTHQUAKES IN THE PUGET LOWLAND

The Puget Lowland is a low-elevation region in the fore-arc of the Cascadia subduction zone (Fig. 1). Geodetic and geologic models of the Cascadia fore-arc show a series of migrating, clockwise-rotating fore-arc blocks driven by Pacific–North America shear and basin-and-range extension (Wells *et al.*, 1998; McCaffrey *et al.*, 2013). Clockwise fore-arc block rotation causes higher rates of convergence in western Washington than elsewhere in Cascadia, because the Oregon coast range block impinges on Tertiary volcanic rocks and sediments in southwest Washington, compressing these Tertiary rocks against the southern edge of the coast range of British Columbia. Global Positioning System measurements indicate several mm/yr of north–south shortening along the fore-arc (Mazzotti *et al.*, 2002). This shortening is accommodated by an array of east-striking reverse faults, northeast-striking dextral-reverse faults, and northwest-striking sinistral-reverse faults cutting the Puget Lowland, which are mapped based on geologic, geophysical, and topographic data (Sherrod and Gomberg, 2014).

Although paleoearthquake scarps are difficult to see from a distance in the landscape due to thick vegetation, the remnants of scarps are quite evident in light detection and ranging (lidar) imagery of the region (e.g., Nelson *et al.*, 2014). Many of the scarps lie on a broad plain of glacial till, deposited when the margin of the Cordilleran ice sheet expanded southward into western Washington during the last glaciation (MIS II). This glacial advance (known as the Vashon Stade of the Fraser Glaciation; Armstrong *et al.*, 1965) and subsequent deglaciation was remarkably rapid, with ice covering the landscape for only ~1020 yr, until deglaciation about 14,500 B.C.E. (Porter and Swanson, 1998). The Vashon till is thick enough to mask older preglacial scarps and similar geomorphic features, so that the total vertical separation observed across a fault scarp is known to be post-14,500 B.C.E. deformation and, in many cases, attributable to specific Holocene earthquakes.

PALEOEARTHQUAKE DATA

We assembled a dataset of 27 paleoearthquakes on 13 active faults in the Puget Lowland and vicinity (Table 1). All of the paleoearthquakes are described in the literature, and offset measurements were taken from those sources.

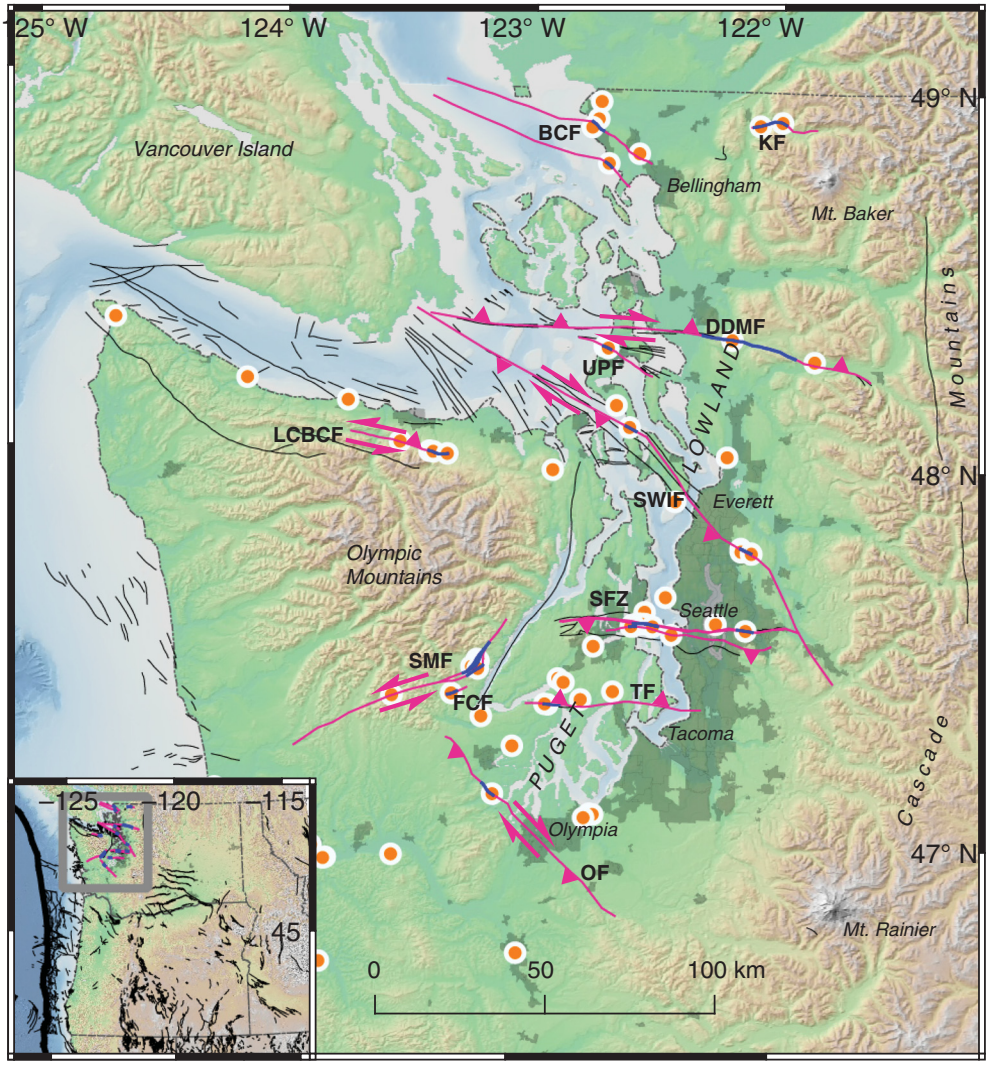

Figure 1. Map of the Puget Lowland. Paleoseismic sites are shown as orange dots. Ruptures studied here are shown in pink and blue; pink represents the maximum possible length of each earthquake, and blue represents the minimum. Additional faults in black are from the U.S. Geological Survey (USGS) Quaternary fault and fold database (see Data and Resources). Shaded areas indicate urban development. Inset shows study area location. BCF, Bellingham Coastal faults; DDMF, Darrington–Devil's Mountain fault; FCF, Frigid Creek fault; KF, Kendall fault; LCBCF, Lake Creek–Boundary Creek fault; OF, Olympia fault; SFZ, Seattle fault zone; SMF, Saddle Mountain faults; SWIF, South Whidbey Island fault zone; TF, Tacoma Fault; UPF, Utsalady Point fault.

Maximum and minimum ruptures were mapped based on previous geomorphic, geophysical, and geological studies, to measure the lengths of the ruptures. The ruptures for each fault were mapped for this study in QGIS (see Data and Resources) on base imagery from lidar, 90 m Shuttle Radar Topographic Mission (Rosen *et al.*, 2000) and bathymetry data from the Global Multi-Resolution Topography data synthesis (Ryan *et al.*, 2009). The locations of the fault traces are based on, and adhere very closely to, published traces in the paleoseismic and other geologic literature, the Washington State geologic map, and the U.S. Geological Survey (USGS) Quaternary fault and fold database (see Data and Resources). However, because our methods require distinct minimum and maximum traces, the existing Geographic Information Systems (GIS) data were not directly suitable, so remapping with our objectives in mind was necessary.

These mapped fault traces, with offset information, fault-specific references, and other information included as metadata, are available as a GIS file in the supplemental material available to this article (see Data and Resources). In general, the maximum rupture lengths are taken as the length of the faults as expressed in bedrock geologic maps, whereas the minimum rupture lengths are the lengths of the scarps (or other paleoseismic surface disruption) observed in the vicinity of the paleoseismic study site.

Comprehensive reviews of the paleoseismic and lidar data for all earthquakes considered here appear in Nelson *et al.* (2014) and Sherrod and Gomberg (2014), with updated study of the Saddle Mountain fault (SMF) zone by Barnett *et al.* (2015). Because these works are recent and thoroughly describe the events studied here, we direct the reader to them for specific details and geologic context beyond what is provided in this work. In particular, the delineation of individual paleoearthquakes at a study site and the correlation of those earthquakes between different sites have been performed in the references listed earlier and those contained therein. No new offset data, correlations, or other interpretations are presented in this work, beyond the maximum and minimum rupture length estimates and improved magnitude estimation that is the focus of our study.

Fault zones and paleoearthquakes

Bellingham Coastal faults. These faults are parallel faults extending from Bellingham northwest for ~50 km. The southeastern extents show short, discontinuous scarps and

TABLE 1
Parameters, References, and Mean Posterior Magnitude $p(M|DL)$ for All Earthquakes in This Study

Earthquake Name	Fault	Offset (m)	Offset Error (m)	Vertical Separation (m)	Vertical Separation Err (m)	Dip (°)	Dip Err (°)	Rake (°)	Rake Err (°)	Minimum Length (km)	Maximm Length (km)	Reference(s)	$p(M\|DL)$ Mean (M)
West_Point_Sewer_Log_Death	Seattle fault zone	—	—	7.00	1.00	45	15	90.0	8	6	71	Atwater and Moore (1992); Bucknam *et al.* (1992); Nelson *et al.* (2003)	7.50
smf_E3	Saddle Mountain East	—	—	5.50	2.50	67	10	67.5	8	11	75	Wilson *et al.* (1979); Witter *et al.* (2008); Barnett *et al.* (2015)	7.27
SWIF_EQ1	SWIFZ	—	—	1.90	1.50	55	30	125.0	8	3	170	Sherrod *et al.* (2008)	7.21
SWIF_EQ2	SWIFZ	—	—	1.50	0.50	60	15	125.0	8	3	170	Kelsey *et al.* (2004)	7.19
DDMFZ_EQ1	Darrington–Devils Mountain fault	2.30	1.10	1.00	—	60	20	166.0	8	28	132	Personius *et al.* (2014)	7.17
RSC5_Death	Olympia	—	—	2.00	1.00	45	15	125.0	8	5	74	Sherrod (2001)	7.11
TFZ_EQ	Tacoma	—	—	3.00	1.00	55	15	90.0	8	4	52	Johnson, Blakely, *et al.* (2004); Sherrod *et al.* (2004)	7.10
smf_E1	Saddle Mountain West	2.15	0.25	—	—	67	10	67.5	8	12	75	Wilson *et al.* (1979); Witter *et al.* (2008)	7.07
smf_E2	Sund Creek–Saddle Mountain East	—	—	1.70	0.30	67	10	67.5	8	5	76	Barnett *et al.* (2015)	7.06
VasaParkEQ	Vasa Park	—	—	1.00	0.50	26	5	90.0	8	4	71	Sherrod (2002)	7.03
sandypt_eqA	Bellingham Coastal faults	—	—	2.00	1.00	45	30	90.0	8	2	64	Kelsey *et al.* (2012)	7.00
Birch_Bay_Uplift	Birch Bay fault	—	—	1.25	0.75	45	30	90.0	8	4	66	Kelsey *et al.* (2012)	6.90
SFZ_EQ_B	Toe Jam	—	—	1.20	0.60	70	10	90.0	8	6	71	Nelson *et al.* (2003)	6.89
SFZ_EQE	Waterman	—	—	1.40	1.00	35	15	90.0	8	2	50	Nelson *et al.* (2014)	6.87
crane_lake_eq_1	Toe Jam	1.25	0.25	1.00	–	70	10	90.0	8	4	53	Nelson *et al.* (2003)	6.85
Utsalady_EQ1	Utsalady Point	—	—	1.50	0.50	60	30	113.5	8	2	25	Johnson, Nelson, *et al.* (2004)	6.77
SFZ_EQ_A	Seattle fault zone	—	—	1.50	1.40	45	15	90.0	8	4	54	Sherrod *et al.* (2000)	6.76
crane_lake_eq_2	Toe Jam	—	—	1.00	0.50	70	10	90.0	8	4	53	Nelson *et al.* (2003)	6.75
kendall_eqA	Kendall	—	—	1.10	0.30	45	15	90.0	8	10	20	Sherrod *et al.* (2013)	6.68
Utsalady_EQ2	Utsalady Point	—	—	1.00	0.30	60	30	113.5	8	2	25	Johnson, Nelson, *et al.* (2004)	6.68
SFZ_EQ_V	Toe Jam–folding	—	—	0.60	0.20	70	10	90.0	8	6	71	Nelson *et al.* (2003)	6.67
LCBC_EQ3	Lake Creek–Boundary Creek	—	—	0.75	0.25	55	5	67.5	8	6	29	Nelson *et al.* (2007)	6.67
kendall_EQB	Kendall	—	—	1.20	0.50	45	15	90.0	8	10	20	Barnett *et al.* (2007); Siedlecki and Schermer (2007); Sherrod *et al.* (2013)	6.66

(*continued*)

TABLE 1 (*Continued*)

Earthquake Name	Fault	Offset (m)	Offset Error (m)	Vertical Separation (m)	Vertical Separation Err (m)	Dip (°)	Dip Err (°)	Rake (°)	Rake Err (°)	Minimum Length (km)	Maximm Length (km)	Reference(s)	*p*(*M*|*DL*) Mean (M)
kendall_EQC	Kendall	—	—	0.55	0.15	45	15	90.0	8	10	20	Barnett *et al.* (2007); Siedlecki and Schermer (2007); Sherrod *et al.* (2013)	6.56
frigid_EQ_1	Frigid Creek	—	—	2.10	0.50	65	15	–90.0	8	3	6	Blakely *et al.* (2009)	6.54
sandypt_eqB	Bellingham Coastal faults	—	—	1.00	0.50	45	30	90.0	8	2	12	Kelsey *et al.* (2012)	6.40
Sandy_Point_EQ_C	Bellingham Coastal faults	—	—	0.50	0.25	45	30	90.0	8	2	12	Kelsey *et al.* (2012)	6.30

SWIFZ, South Whidbey Island fault zone.

lineaments in lidar data, and the entire faults are evident in geophysical imagery extending northwest through the Straits of Georgia. Studies show three parallel faults, namely, the Drayton Harbor, Birch Bay, and Sandy Point faults. Coastal geomorphology and trenching across the scarps yield evidence for four Holocene earthquakes with 0.5–2 m vertical separation (Kelsey *et al.*, 2012). Evidence for lateral displacement is lacking, so the earthquakes are interpreted as reverse events on faults with dips ranging from 15° to 75°.

Kendall (Boulder Creek) fault. The Kendall or Boulder Creek fault is a short, sinuous fault in the northwestern Cascades east of Bellingham (Barnett *et al.*, 2007; Siedlecki and Schermer, 2007; Sherrod *et al.*, 2013). Scarps are evident in the lidar for the western half of the fault zone, but bedrock faulting continues on trend for several kilometers eastward before splaying north and south (Sherrod *et al.*, 2013); however, the Nooksack River flows along the fault and may have removed evidence of Quaternary deformation. Three paleoearthquakes have been described from trenches along the scarp. These are all taken to be reverse events with 0.5–1 m vertical separations on a moderately dipping fault (Barnett *et al.*, 2007; Siedlecki and Schermer, 2007; Sherrod *et al.*, 2013).

Darrington–Devil's Mountain fault. The Darrington–Devil's Mountain fault strikes east from the western Cascades, across northern Whidbey Island and into the Strait of Juan de Fuca, where it is interpreted in geophysical data; at its western end, it appears to merge with the South Whidbey Island fault and the Leech River fault near the city of Victoria on Vancouver Island. The structure has a protracted history, with evidence for both right-reverse and left-reverse slips at different times in the Cenozoic. The most recent work on the fault, by Personius *et al.* (2014), has documented one unambiguous Holocene earthquake with dominantly right-oblique slip of 2.2 ± 1.1 m on a steeply dipping plane; the dip-slip component is inferred to be reverse, based largely on local and regional focal mechanisms, geodesy, and the general tectonics of the Cascadia fore-arc; however, some ambiguity exists based on the fault geology, and other workers have interpreted the opposite sense of slip (e.g., Johnson *et al.*, 2001; Dragovich and DeOme, 2006). (The sense of slip does not affect the estimated magnitudes in this work, as the scaling relationships between magnitude and rupture characteristics that we use do not incorporate sense of slip.) Personius *et al.* (2014) estimated a minimum rupture length of 30 km based on discontinuous scarps across the best-preserved section the fault (which is still cut by numerous streams and under several lakes); however, the rest of the fault is located in zones of poor preservation potential or undersea, so ruptures may be much longer.

Utsalady Point fault. The Utsalady Point fault zone is a short, northwest-striking, multistranded fault crossing

Whidbey Island, a few kilometers south of the Darrington–Devil's Mountain fault, and is likely a splay off of the latter fault. Johnson, Nelson, *et al.* (2004) found evidence for two paleoearthquakes through trenching and lidar mapping of the subaerial trace of the fault. These earthquakes are interpreted as left-reverse, with ~1 m of vertical separation and 2.2 m of left-lateral separation for the more recent event (~1550–1850 C.E.), and ~1 m vertical separation for an older event with an unknown amount of lateral offset; dip is variable in the trenches, but the principal displacement zone appears to be rather steeply dipping. The scarp height is larger than the cumulative vertical separation in the trenches, which could result from either off-fault deformation (i.e., shallow folding) or deformation that predates the oldest stratigraphic units in the trenches. For simplicity, we treat both earthquakes as having the same rake and uncertainty.

South Whidbey Island fault zone. The South Whidbey Island fault zone is a long, northwest-striking structure that extends from just east of Vancouver Island southwest to the Cascades foothills east of Seattle, about 170 km. Investigations at several points along the fault yield evidence of at least four late-Quaternary earthquakes, but only two events have measurable displacement. The more recent event is the best recorded as shorelines from central Whidbey Island uplifted differentially by 1–2 m (Kelsey *et al.*, 2004) from an event 1250–920 B.C.E. Faulting on the mainland ~70 km to the southwest is dated as slightly younger but is possibly the same event (Sherrod *et al.*, 2004). A much older (late Pleistocene to earliest Holocene) paleoearthquake is inferred at the latter site, with ~2 m vertical separation (Sherrod *et al.*, 2008).

Seattle fault zone (SFZ). The SFZ is a somewhat complex set of east-striking reverse faults that place Tertiary volcanic rocks in the south above the Neogene–Quaternary Seattle basin to the north, although, some shallow strands are north-side-up and are interpreted as back thrusts (e.g., Nelson *et al.*, 2003). The paleoseismic work on the fault to date shows it as the most active fault zone in the Cascadia fore-arc, with eight large events since deglaciation. These paleoearthquakes are observed at the surface on several different strands that are often anastomosing. The different traces are thought to be splays that merge on the same south-dipping structure within the seismogenic crust, based on seismic imaging studies (e.g., Brocher *et al.*, 2001; ten Brink *et al.*, 2002) and geologic cross sections (e.g., Nelson *et al.*, 2003; Kelsey *et al.*, 2008). Trenches across one of these back thrusts, the Toe Jam Hill fault, have yielded the clearest evidence for paleoearthquakes, four events with vertical separations ranging from 0.6 to 1.2 m; the fault geometry here is steep (70° ± 10°), so these values are similar to the total offset. Trenches across shallower, south-dipping faults have produced evidence for similar vertical separations (Sherrod, 2002; Nelson *et al.*, 2014).

Shorelines south of the fault traces have been uplifted by as much as 7 ± 1 m in a single event ~850 C.E. (Bucknam *et al.*, 1992), which produced a tsunami in Puget Sound (Atwater and Moore, 1992), although no single scarp has been identified. Modeling of the uplifted shorelines and tsunami deposits from this earthquake suggests rupture of a north-dipping roof ramp composed of several, mostly blind back thrusts, merging with a moderately south-dipping main reverse fault at a few kilometers depth (e.g., ten Brink *et al.*, 2006; Pratt *et al.*, 2015) and a magnitude of $\mathbf{M} \sim 7.5$ (ten Brink *et al.*, 2006). Because the accumulated geologic, geophysical, and tectonic geomorphologic observations suggest that the complexity in the SFZ is largely near surface, we do not attempt to include down-dip geometric variation of the fault in our study, and, instead, consider each earthquake to occur on a plane with the stated dip.

SMF zone. The SMF zone is a narrow, anastomosing fault zone that strikes northeast on the southern margin of the Olympic Mountains. The fault's northeasternmost extent is within 15 km of the western SFZ, and, to the southwest, it may merge with the Canyon River fault (Walsh and Logan, 2007), as represented by the maximum rupture in Figure 1. Paleoseismic investigations on this fault have recovered evidence of three earthquakes on three nearby strands of the fault (Wilson *et al.*, 1979; Witter *et al.*, 2008; Barnett *et al.*, 2015), where it splits at a releasing bend (Fig. 1). Two of these earthquakes have produced left-reverse offsets that are fairly typical for the region (~1.5–2.5 m), but, one is much larger, with vertical separation of up to 8 m measured with lidar (Barnett *et al.*, 2015). Incidentally, this high-slip earthquake has overlapping time constraints with the high-uplift Seattle fault event about 1100 yr ago, raising the possibility that one of these events was triggered by the other, or even that they represent a single multifault rupture. The maximum lengths of ruptures on the SMF zone are interpreted to link to the Canyon River fault, given the large magnitude of offset.

Frigid Creek fault. The Frigid Creek fault is a short (<10 km) fault, with a north-side-up scarp located 4 km south of the SMF zone. Excavations across the scarp indicate about 2.5 m of vertical separation across a south-dipping normal fault, which is thought to represent a single event (Blakely *et al.*, 2009).

Tacoma fault. The Tacoma fault is thought to be a north-dipping reverse fault based on interpretations of geophysical data, raised shorelines and tidal platforms, and a few preserved scarps (Johnson, Blakely, *et al.*, 2004; Sherrod *et al.*, 2004). The geomorphic evidence for Holocene uplift of the fault suggests a single event with 3 ± 1 m of vertical on the western extent of the fault separation (Sherrod *et al.*, 2004), although, approximately, 350–400 m of Quaternary uplift of the hanging wall is interpreted all along the fault (Johnson, Blakely, *et al.*, 2004), suggesting it is active along its entire length.

Olympia fault. The Olympia fault is a significant bedrock structure that bounds the southwestern Tacoma basin, bringing Eocene volcanic rocks in the hanging wall north and over the Tertiary basin sediments; however, the fault does not clearly break the surface of the thick late-Quaternary sediments in the Puget Lowland. Evidence for Holocene seismic activity is based on submerged forests and uplifted marsh soils, indicative of rapid differential changes in sea level of up to 4 m across the fault at several locations (Sherrod, 2001).

Lake Creek–Boundary Creek fault. The Lake Creek–Boundary Creek fault is a north-dipping dextral-reverse fault on the northern margin of the Olympic Mountains (e.g., Schasse and Wegmann, 2000). Lidar mapping and trenching has confirmed at least one Holocene earthquake with limited vertical separation (0.5–1 m), but scarps are preserved in places along the rugged fault trace over at least 30 km (Nelson *et al.*, 2007, 2017). Scarp-facing direction is not consistent along the fault length, suggesting that dextral displacement is dominant and scarp facing may be locally related to positive and negative flower structures (Nelson *et al.*, 2007).

Rupture lengths

Rupture lengths for each earthquake were not measured precisely, as each of the probable ruptures crosses heavily vegetated, urbanized, and/or submarine zones. In addition, most of the studied faults have had multiple earthquakes in the Holocene, so observed faults scarps are cumulative scarps, and the lengths of individual earthquakes cannot be directly measured. Furthermore, although scarps are evident in the lidar data for most of these faults (e.g., Nelson *et al.*, 2014), the scarps are largely very short and discontinuous, due to the environmental conditions disfavoring preservation; this prevents using the scarp lengths to approximate rupture length or taking multiple measurements of offset at different locations along the faults to better constrain offset distributions (e.g., Hemphill-Haley and Weldon, 1999).

Therefore, we bracketed rupture length by maxima and minima. The maxima are essentially the full length of each fault zone determined from geological and geophysical data. Many of the faults studied are shown geologically to be confined to the Puget Lowland, and do not extend far into the marginal Cascade and Olympic mountains. A few may cut through the Cascades and into Yakima Fold Province farther east (Blakely *et al.*, 2011), but there is no documented Quaternary fault activity in the Cascades. The minima are the lengths between paleoseismic trenches in which the earthquakes are observed, or the lengths of clear ruptures in topographic data.

Rupture-length estimates vary from short to moderate lengths: $L_{\min}$ ranges from 2 to 33 km (median 4 km), whereas $L_{\max}$ ranges from 6 to 186 km (median 53 km). The median $L_{\max} : L_{\min}$ ratio is 11.8, and the mean is 13.8.

Offset measurements

Paleoearthquake offsets were measured in trenches, coastal marsh stratigraphy, shoreline terraces, field surveys, or lidar scarp profiling. Measured fault separations (which are primarily vertical) range from 0.5 ± 0.25 to 7.0 ± 1.0 m, corresponding to ~0.5–14 m total fault offset (near-surface fault dips are generally steep). The median offset is 2.1 m. Vertical separations were converted to net offsets using fault dip and rake estimates (e.g., Meghraoui *et al.*, 1988). Uncertainties were estimated for offset, dip, and rake, and were treated as uniform distributions and propagated through final offset distributions using Monte Carlo simulations. However, the offset distributions produced from Monte Carlo simulations were not generally uniform, because of the nonlinearities in the trigonometric functions used to convert vertical separation to offset.

Length-offset scaling

Earthquakes in the Puget Lowland have rupture lengths that are limited by the lengths of the faults that host them. Geological mapping and potential field surveys show that several reverse faults, such as the SFZ, do not extend into the mountains bounding the eastern and western margins of the lowland. However, observed offsets for individual events may be quite large: Vertical offsets of up to 8 m have been measured from uplifted shorelines and fault scarps on lidar (Sherrod *et al.*, 2000; Nelson *et al.*, 2014; Barnett *et al.*, 2015), although most offset measurements are between 1 and 2.5 m.

Even moderate observed offsets show ratios of offset to maximum rupture length that are higher than that predicted by the empirical scaling relationships between mean offset and rupture length for faults of all rupture types (e.g., Wells and Coppersmith, 1994), though the scaling is typical for continental reverse-fault ruptures (Wesnousky, 2008), despite some of these ruptures being oblique slip (Fig. 2). Because earthquake magnitude is proportional to the product of displacement and length (Aki and Richards, 1980), predictions of earthquake magnitude based on either rupture length or displacement will only be accurate if the length to displacement ratio is typical for the data used to construct the scaling. If the ratio is atypical, the use of a single data type will bias the predicted earthquake magnitude.

PALEOEARTHQUAKE MAGNITUDE INVERSION

Earthquake magnitude given displacement

We use rupture length information to aid in paleoearthquake magnitude estimation by extending the Bayesian magnitude inversion scheme developed by Biasi and Weldon (2006). Their method is centered around Bayes' theorem cast appropriately for this problem:

$$p(M|D) = p(M)\frac{p(D|M)}{p(D)}, \tag{1}$$

in which $p(M)$ is the prior probability of the earthquake magnitude M, $p(D|M)$ is the likelihood function, which states the likelihood of observing a displacement of size D given an earthquake of magnitude M, and $p(D)$ is the probability of D, which in this case is essentially a normalization constant. The solution to the Bayesian inversion is $p(M|D)$, the posterior magnitude distribution, given the displacement observations.

The likelihood function $p(D|M)$ incorporates the intrinsic variability in the surface displacements at any point in an earthquake surface rupture. This may not be derived simply from first principles (given our current knowledge of earthquake physics). Instead, Biasi and Weldon (2006) derived a likelihood function that incorporates a statistical distribution of normalized surface displacements (which we call $p(D_n)$), and a scaling relationship between earthquake magnitude M and mean surface displacement. $p(D_n)$ is simply an empirical distribution of the frequency (or probability) of an offset D occurring anywhere along the length of an individual rupture divided by the mean displacement for that event; it was made through compilation of 13 well-mapped ruptures. $D_{\text{pred}}(M)$ is the predicted mean surface displacement for a given earthquake magnitude, in our case, from the empirical scaling relationship of Biasi and Weldon (2006). The likelihood function $p(D|M)$ is then constructed as

$$p(D|M) = p(D_n)/D_{\text{pred}}(M). \quad (2)$$

We follow this approach, with a few modifications of the likelihood functions. The first, more minor, modification pertains to the aggregation of the data into $p(D_n)$. Biasi and Weldon (2006) used histograms of the normalized earthquake slip data to represent the earthquake slip distribution, leading to a somewhat noisy function with resolution limited to the histogram bin size (i.e., 0.1 M). We instead use a Gaussian kernel density estimate of the normalized slip data to yield a continuous, smooth distribution function with arbitrary resolution (the bandwidth for the kernel density estimate was chosen automatically through the "Scott rule," Scott, 1992, a commonly used algorithm for data-driven bandwidth selection). The differences are minor (Fig. 3).

The second modification is a bit more significant and reflects the nature of the paleoseismic sampling strategies in their work versus ours. Biasi and Weldon (2006) are concerned primarily about strike-slip ruptures (specifically on the southern San Andreas fault), in which paleoseismic sampling is performed in areas where the geomorphology is favorable for steady sedimentation that will preserve earthquakes in the stratigraphic record. Preservation is presumed independent of the relative magnitude of displacement at the sample site for any given rupture; therefore, their methods assume that the measured displacement at a site is randomly selected along the rupture.

The paleoseismic data used in this work, however, are from dip-slip and oblique-slip faults, and are generally located where

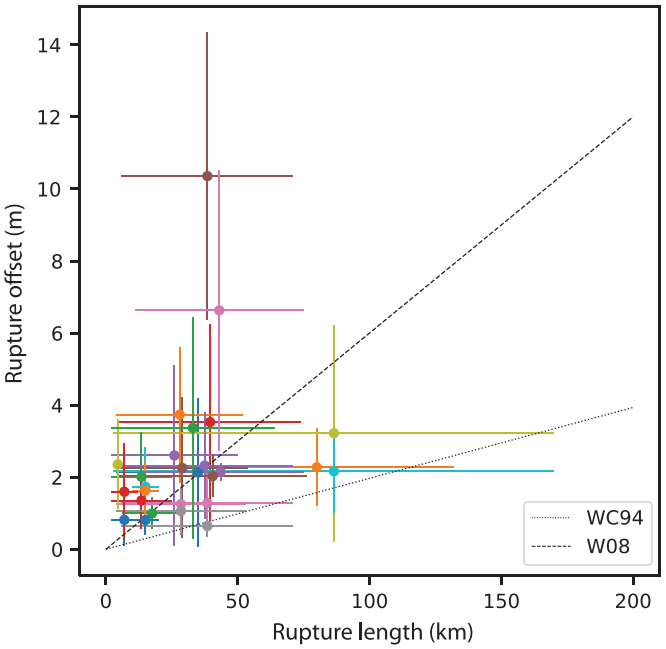

Figure 2. Length-offset scaling for Puget Lowland earthquakes and scaling relationships. WC94, scaling of Wells and Coppersmith (1994) for all earthquakes and W08, scaling of Wesnousky (2008) for continental reverse faults. The different colors are not significant but are to aid in distinguishing data.

scarps are the best preserved in the landscape. Although, the degree of preservation at any point along a scarp may be most influenced by the local environment (i.e., whether the point is in an active stream channel, under the sea, in a flat forest, etc.), it will also be influenced by the size of the scarp at that point: sites with larger offsets are more likely to be preserved in the landscape and are more likely to attract the attention of paleoseismologists, all else being equal. This can lead to a bias in sampling (measuring) the offsets, such that points along a rupture with higher offset are more likely to be sampled than sites with lower offset. This implies that sampling is not performed randomly along the rupture, independent of the local offset amount, and is not fully consistent with the assumptions in the likelihood function of Biasi and Weldon (2006).

Therefore, we introduce a correction into the function $p(D_n)$, so that the probability of sampling at any point along the rupture is proportional to the relative magnitude of the offset of that point; that is, for a rupture with a mean slip of 1 m, a point with 3 m of offset is three times more likely than the mean to be sampled, and a point with 0.5 m of slip is half as likely to be sampled as the mean point. This function is a probability density function (PDF) of the normalized displacement variable (offset/mean offset) that increases linearly from zero at offset = 0 to a relative probability of 4 at four times the mean offset. This function is then normalized to integrate to 1 and then multiplied by the original probability function $p(D_n)$.

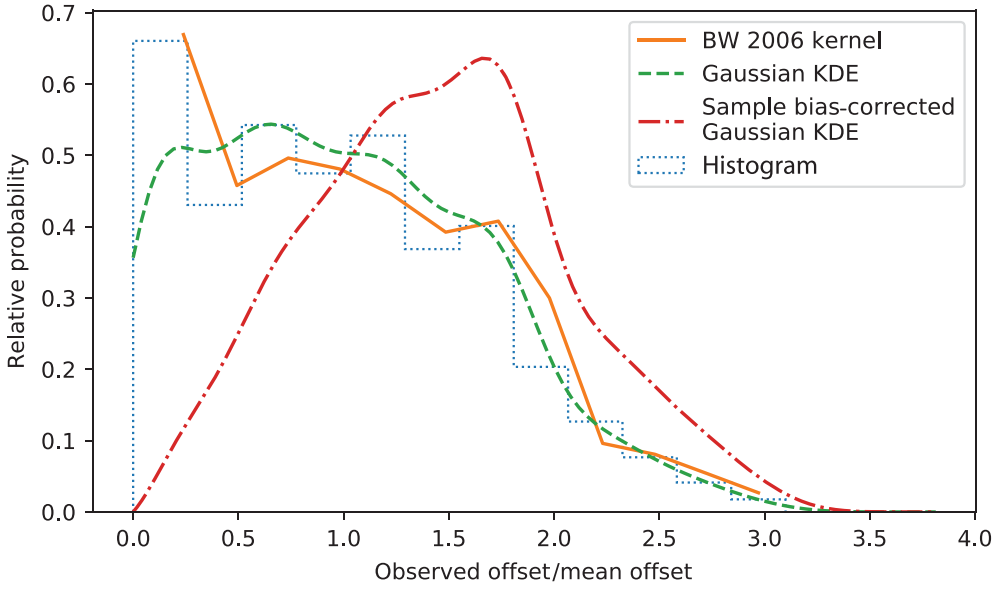

Figure 3. Relative probability distributions of slip magnitude for a rupture (observed slip) relative to the mean slip for that rupture. High probabilities at low relative offset values increase the statistical likelihood that the mean slip of an event was much greater than the observed offset, whereas high probabilities at high relative offset values increase the statistical likelihood that the mean slip was lower than the observed offset. BW 2006 is the kernel from Biasi and Weldon (2006). KDE, Kernel density estimate.

The net effect of this correction is that it reduces the likelihood within the statistical model that a trench (or other measurement site) is located on a part of the scarp that has a much smaller offset than the mean offset for that event, and increases the likelihood that the measurement was taken from a site with a higher-than-average offset.

A more complicated sampling bias correction could be applied that incorporates scarp diffusion modeling, for example, or considers each fault on a case-by-case basis and evaluates the number of sites with potential offset measurements and the preservation potential across the fault length, and could yield more accurate results. However, given the small amount of scarp preserved and the challenging and heterogeneous environment, we feel that a very simple approach is the best here.

Finally, we also extend this method by incorporating uncertainty in offset measurements into the inversion, using Monte Carlo methods. A distribution is defined for the offset measurements, and some large number of samples are drawn randomly from that distribution. Then, the inversion is run for each of those samples (using the same prior) and the posteriors are then averaged to yield a final $p(M|D)$ PDF that incorporates the uncertainty in the offset data.

Length incorporation

We extend the Bayesian framework to include rupture length, by creating an additional likelihood function for the earthquake magnitude based on the rupture length. We use an empirical length–magnitude scaling relationship, to derive magnitude estimates from rupture length:

$$p(L|M) = a + b\log_{10}(L), \tag{3}$$

in which a and b are constants. We use $a = 5.45 \pm 0.08$ and $b = 0.95 \pm 0.06$ (uncertainties are standard error) (Stirling *et al.*, 2002), but updated or problem-specific relations could work as well. We note that this scaling relation is derived from a compilation of global observations; it may be that the Puget Lowlands earthquakes are outliers relative to the global mean, perhaps due to a greater-than-average seismogenic thickness, although, crustal seismicity in the region is generally limited to depths above 25–30 km (Van Wagoner *et al.*, 2002), which is not atypical for fore-arc regions, which are well represented in the data used in the regressions by Stirling *et al.* (2002).

The stated uncertainty in a and b, as well as the wider range between L_{min} and L_{max}, is incorporated through Monte Carlo simulations: for each of n iterations, L is sampled uniformly from (L_{min}, L_{max}), and a and b are sampled from normal distributions with their standard errors. This results in a set of n samples of M, which are then converted to the likelihood function $p(L|M)$ through a kernel density estimation.

We then use $p(L|M)$ to recover the posterior magnitude $p(M|D, L)$ with the equation

$$p(M|D, L) = p(M)p(L|M)\frac{p(D|M)}{p(D)}. \tag{4}$$

An example of this calculation is shown in Figure 4.

An alternative formulation could incorporate both L and the down-dip width W of the fault calculated from estimates of the average fault dip and the seismogenic thickness of the crust to compute the fault area A, and then use regressions of M versus A (e.g., Wells and Coppersmith, 1994; Stirling *et al.*, 2002) or between surface displacement D and mean displacement D_{mean} to calculate the seismic moment M_o for each event as $M_o = \mu A D_{mean}$, in which μ is the shear modulus of the crust (e.g., Aki and Richards, 1980). However, we do not use this method because of the uncertainty in the geometry of the faults at depth, including the down-dip extent of individual large

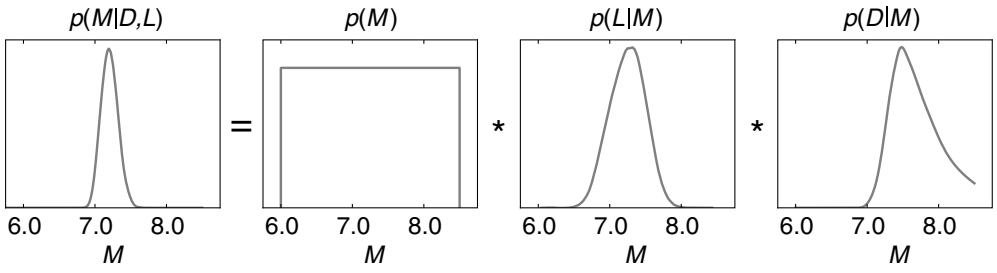

Figure 4. Schematic diagram of equation (4) for an earthquake.

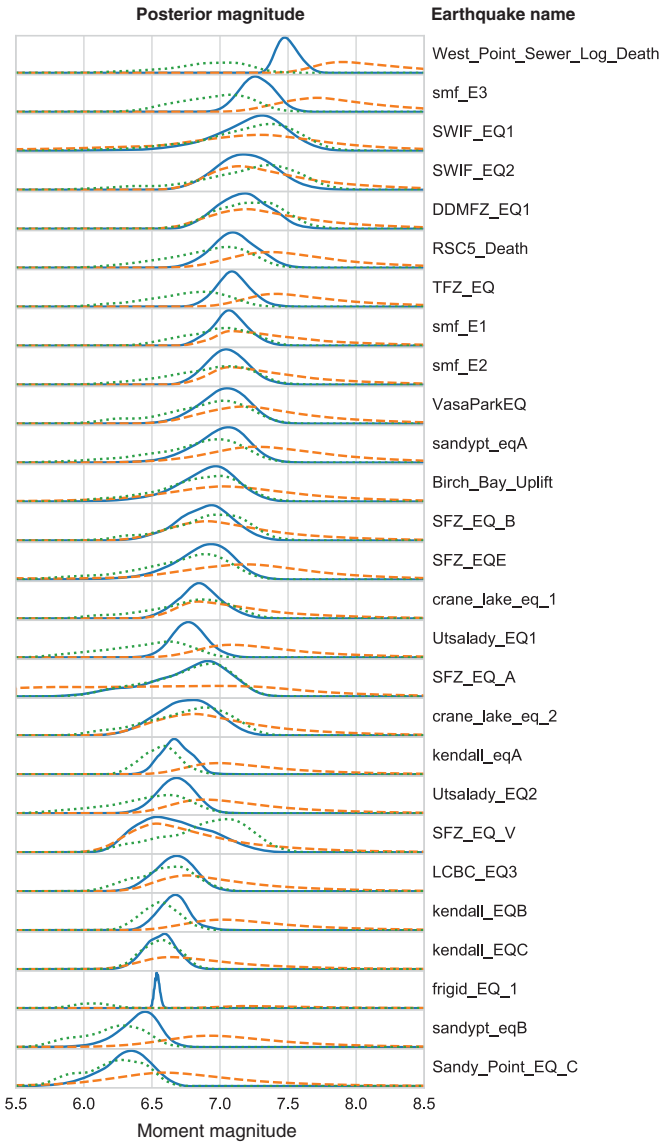

Figure 5. Posterior magnitudes $p(M|D,L)$ (blue lines), $p(M|D)$ (orange-dashed lines), and $p(M|L)$ (green dotted lines) for all events, with their unique event name.

ruptures, the dips of the faults, and any additional geometric complexities, such as those suggested by Brocher *et al.* (2004).

RESULTS AND DISCUSSION

Magnitudes of Puget Lowland paleoearthquakes

Individual paleoearthquakes in the Puget Lowland have posterior magnitudes between 6.3 and 7.5, given both offset and rupture length data (Figs. 5–7 and Tables 1 and 2). In general, the larger earthquakes are less common, although, there are relatively few earthquakes below **M** 6.5, consistent with previous observations that **M** 6.5 and smaller events frequently do not break the surface (e.g., Fialko *et al.*, 2005). Nine of the events have mean $p(M|D,L)$ between 7.0 and 7.5, 15 between 6.5 and 7.0, and three between 6.0 and 6.5.

Effects of length incorporation

Incorporating length into the magnitude inversion substantially reduced both the posterior magnitudes and the uncertainty in the magnitudes. $p(M|D,L)$ was about 0.4 M smaller than $p(M|D)$ for the same event, on average. The uncertainty in each estimate is fairly represented by the interquartile range (IQR, the distance between the 25th and 75th percentiles); the IQR of $p(M|D)$ is, on average, about twice the IQR of $p(M|D,L)$ for a given earthquake (Fig. 7).

In addition, the characteristic shape of the $p(M|D)$ PDF has a right skew (Fig. 6a), with a long, high-M tail (relating to the possibility that the offset measurement occurred on a section of rupture with an offset much lower than the mean offset), although, $p(M|D,L)$ is more symmetrical (Fig. 6b). In this analysis, $p(M)$ extended to M 8.5, and $p(M|D)$ for several events are nonnegligibly truncated at this limit. However, for no events did $p(M|D,L)$ reach **M** 8.0. This is an effect of limiting the rupture length; given empirical global scaling relationships between L, D, and M for strike slip and events, it is very improbable that an **M** 8.0 could occur on faults with total lengths as short as in our dataset. Given the geological controls on fault dimensions, upper magnitude limit is highly unlikely to be simply an underestimation of the possible rupture dimensions, unlike a scenario involving a floating rupture on a >1000 km long strike-slip fault such as the Altyn Tagh fault (e.g., Wang *et al.*, 1997) or Sagaing fault (e.g., Vigny *et al.*, 2003).

One instance in which it is possible that the rupture could be longer than our maximum is if the Saddle Mountain and SFZ ruptured in a single event. This is possible, given the estimated timing of the paleoearthquakes: the Restoration Point

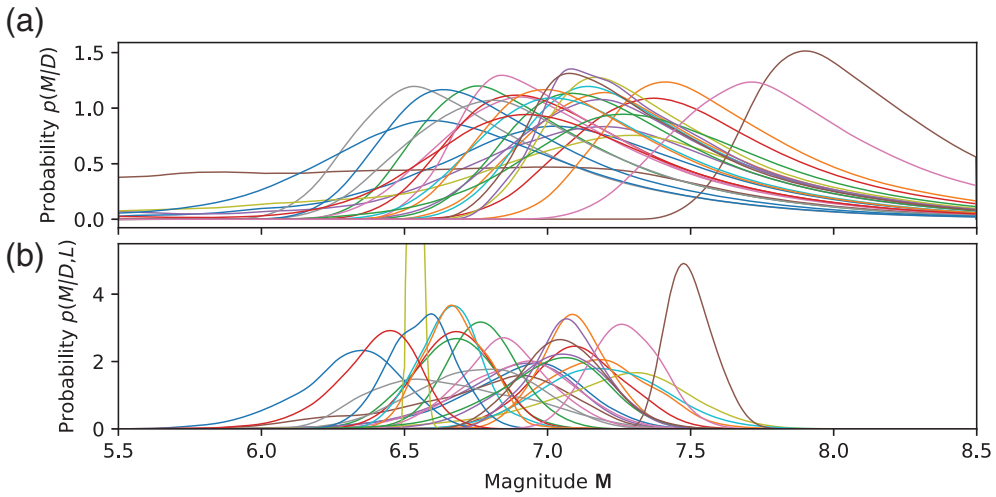

Figure 6. Posterior magnitude probability density functions (PDFs) for Puget Lowland earthquakes. (a) $p(M|D)$ and (b) $p(M|D, L)$.

earthquake occurred about 900–930 C.E., the Saddle Mountain east fault ruptured between 790 and 1640 C.E., and the Saddle Mountain west fault ruptured between 750 and 980 C.E. (Sherrod *et al.*, 2000; Nelson *et al.*, 2003; Witter *et al.*, 2008; Barnett *et al.*, 2015) (these two Saddle Mountain ruptures are considered the same event in this work). These faults have geometries and kinematics that are not incompatible: The SMF strikes ~60° and is reverse sinistral, whereas the SFZ strikes ~90° and is reverse. The surface traces, as we have mapped them, come to within about 13 km of each other, which is a greater distance than the 5 km upper limit in the Uniform California Earthquake Rupture Forecast, version 3 multifault model, but a shorter distance than observed rupture gaps in the 2008 Wenchuan, China (Zhang *et al.*, 2011) and 2016 Kaikoura, New Zealand (Hamling *et al.*, 2017) earthquakes. These faults have not been demonstrated to link at depth, although, this has been suggested by Blakely *et al.* (2009), based on interpretation of geological and geophysical data. Furthermore, both of these events show much larger offsets than the rest in our dataset: a mean of 10.2 m on the SFZ and 6.7 m on the SMF. (The values in Table 1 are observations of vertical separation, whereas the offsets listed here are net fault slip.) Simultaneous rupture of >5 m on separate faults with such different strikes and rakes has not been observed, although the Wenchuan (Zhang *et al.*, 2011) and Kaikoura earthquakes (Hamling *et al.*, 2017), both $M \sim 7.8$–7.9, are close enough to demonstrate the possibility. The total rupture length of this event would be ~70–150 km, and cursory analysis indicates a most-likely magnitude of 7.8, though the PDF extends to M 8.3.

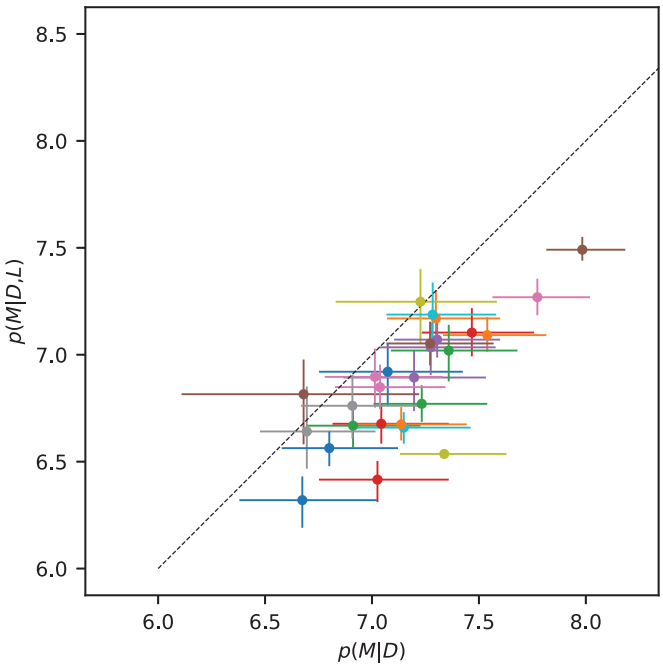

Figure 7. Scatterplot comparing $p(M|D)$ and $p(M|D, L)$ for each event. Points represent the median for each posterior PDF, and error bars represent the 25th and 75th percentiles. Earthquakes that plot below the black-dashed line have had posterior magnitudes reduced by the incorporation of length data into the magnitude inversions.

Implications for Puget Lowland seismic hazard

The paleoearthquake magnitudes resulting from this analysis generally compare well with the expected earthquakes from fault and crustal area sources in the Puget Lowland region of the NSHM. Seismic sources in this region include an area source centered over Puget Sound that produces earthquakes of up to M 7.3 and several discrete fault sources. The magnitude estimates from faults in this dataset are copacetic with the maximum or characteristic earthquake magnitudes in the NSHM, with a few exceptions. The largest paleoearthquake in the dataset, the 900 C.E. **M** 7.5 Restoration Point event on the Seattle fault, is somewhat larger than the maximum magnitude for that structure in the NSHM, M 7.2 (Frankel *et al.*, 2002), which is based on fault length alone; this earthquake is shown to have uplifted shorelines up to 8 m vertically over much of its length, indicating an uncommonly high amount of single-event displacement for any earthquake not on a megathrust. However, our calculated magnitude is only

TABLE 2
Percentiles for Posterior Earthquake Magnitude *p(M|DL)* for All Earthquakes in This Study

Earthquake	5%	25%	50%	75%	95%
Birch_Bay_Uplift	6.473	6.761	6.920	7.053	7.233
DDMFZ_EQ1	6.863	7.038	7.170	7.302	7.482
LCBC_EQ3	6.413	6.566	6.668	6.767	6.899
RSC5_Death	6.827	6.992	7.104	7.218	7.386
SFZ_EQE	6.458	6.737	6.893	7.023	7.191
SFZ_EQ_A	6.182	6.581	6.815	6.977	7.170
SFZ_EQ_B	6.530	6.752	6.896	7.029	7.212
SFZ_EQ_V	6.281	6.467	6.641	6.851	7.122
SWIF_EQ1	6.686	7.053	7.248	7.401	7.608
SWIF_EQ2	6.839	7.044	7.188	7.338	7.548
Sandy_Point_EQ_C	5.959	6.191	6.320	6.431	6.575
TFZ_EQ	6.893	7.014	7.092	7.176	7.308
Utsalady_EQ1	6.563	6.686	6.770	6.857	6.992
Utsalady_EQ2	6.446	6.584	6.677	6.767	6.896
VasaParkEQ	6.710	6.905	7.035	7.152	7.305
West_Point_Sewer_Log_Death	7.377	7.440	7.491	7.551	7.644
crane_lake_eq_1	6.590	6.746	6.848	6.953	7.122
crane_lake_eq_2	6.395	6.608	6.761	6.905	7.092
frigid_EQ_1	6.506	6.524	6.536	6.551	6.569
kendall_EQB	6.470	6.584	6.659	6.731	6.851
kendall_EQC	6.362	6.479	6.563	6.641	6.752
kendall_eqA	6.497	6.599	6.674	6.755	6.860
sandypt_eqA	6.635	6.875	7.020	7.140	7.299
sandypt_eqB	6.119	6.311	6.416	6.503	6.617
smf_E1	6.851	6.986	7.071	7.158	7.296
smf_E2	6.809	6.950	7.053	7.155	7.308
smf_E3	7.068	7.185	7.269	7.356	7.476

marginally higher than the maximum magnitude produced by the area source. In the NSHM, the South Whidbey Island fault zone is given a maximum magnitude of 7.4, based on its great length (168 km), but measured vertical separations on the fault are less than 2 m (Kelsey *et al.*, 2004; Sherrod *et al.*, 2008), which pull the most-likely paleoearthquake magnitudes in this study to 7.2.

In addition, the reduction in the uncertainty of the posterior $p(M|D, L)$ paleoearthquake estimates, relative to $p(M|D)$, increases the consistency between the paleoseismic data and the seismic sources in the NSHM. This is because the large displacements typical of Puget Lowlands earthquakes yield, particularly high "right" tails, with appreciable probability for almost all events at **M** 7.5; for the highest-displacement events, the right tails approach or exceed M 8 (Fig. 5). These tails are greatly diminished in the $p(M|D, L)$ estimates, both due to the incorporation of rupture length and to the sample bias correction.

However, the earthquakes studied here, although representing a mostly complete record of surface-breaking earthquakes in the Puget Lowland, are far from the only source of regional seismic hazard, as the area is above the Cascadia subduction zone. The reduction in earthquake magnitude given here only concerns these shallow, upper-plate events and does not modify hazard estimates from Cascadia at all (including moderate-depth in-slab seismicity directly below the crustal faults studied here).

CONCLUSIONS

We present statistical methods to estimate paleoearthquake magnitude by a joint Bayesian regression of rupture offset and length, and derive estimates for the magnitude of 27 paleoearthquakes in the Puget Lowland region of Washington; these are between **M** 6.3 and 7.5. The use of rupture length in the inversion increases the precision and decreases the magnitudes of the posterior magnitude estimates $p(M|D, L)$ relative to $p(M, D)$, which only incorporates offset measurements, in spite of the factor of 10 uncertainty in the length estimates. This is largely because the maximum allowable rupture lengths are quite short relative to the offsets. The methods presented here are general and easily applied to paleoseismic datasets in a range of geographic and tectonic regimes.

DATA AND RESOURCES

Several datasets were used in this work; paleoseismic offset data and original fault mapping are all from published work, as discussed earlier. The remapped ruptures (minimum and maximum lengths) and published offset data are found in a public GitHub repository (https://github.com/cossatot/puget_sound_paleomagnitude_manuscript, last

accessed January 2019), as a GeoJSON (plain text vector Geographic Information Systems [GIS]) file. This repository also contains a Python script to run the calculations and to produce the figures showing results. Both the GIS file and the Python script are included in the supplemental material as well. Detailed mapping was performed on light detection and ranging (lidar) data from the Puget Sound Lidar Consortium (http://pugetsoundlidar.ess.washington.edu, last accessed January 2019). Mapping was done using QGIS (www.qgis.org, last accessed November 2020). The U.S. Geological Survey (USGS) Quaternary fault and fold database (https://pubs.usgs.gov/fs/2004/3033/fs-2004-3033.html, last accessed November 2020) is shown in Figure 1. Code to perform similar calculations is incorporated into *culpable*, an open-source Python library for various fault-related calculations (https://github.com/cossatot/culpable/, last accessed January 2019). The paleoearthquake magnitude calculations rely heavily on the *NumPy* (Oliphant, 2007; van der Walt *et al.*, 2011), *SciPy* (www.scipy.org, last accessed January 2019), and *Pandas* (McKinney, 2010) packages. Information and simple examples on using the *culpable* library, to perform these calculations with other data, are found at the provided URL.

ACKNOWLEDGMENTS

The authors thank many paleoseismologists, marine geophysicists, and other geoscientists who have worked to produce the rich paleoseismic catalog for the Puget Lowland. The authors also thank two anonymous external reviewers and Thomas Brocher and Glenn Biasi for their internal U.S. Geological Survey (USGS) reviews, which improved this article, and Mark Stirling for his editorial guidance. G. Biasi is also thanked for additional discussion on the sampling biases of paleoseismic sites on dip-slip faults.

REFERENCES

Aki, K., and P. G. Richards (1980). *Quantitative Seismology: Theory and Methods*, W. H. Freeman, New York, New York.

Armstrong, J. E., D. R. Crandell, D. J. Easterbrook, and J. B. Noble (1965). Late Pleistocene stratigraphy and chronology in southwestern British Columbia and northwestern Washington, *Geol. Soc. Am. Bull.* **76,** no. 3, 321–330, doi: 10.1130/0016-7606(1965)76[321:LPSACI]2.0.CO;2.

Atwater, B. F., and A. L. Moore (1992). A tsunami about 1000 years ago in Puget Sound, Washington, *Science* **258,** no. 5088, 1614–1617, doi: 10.1126/science.258.5088.1614.

Barnett, E., H. M. Kelsey, B. L. Sherrod, J. Hughes, E. R. Schermer, R. Haugerud, C. Weaver, E. Siedlecki, and R. Blakely (2007). Active faulting at the northeast margin of the Greater Puget Lowland: A trenching and wetland coring study of the Kendall fault scarp, Whatcom County, northwest Washington, *GSA Cordilleran One Hundred and Third Meeting*, Bellingham, Washington, 22–25.

Barnett, E. A., B. L. Sherrod, J. F. Hughes, H. M. Kelsey, J. L. Czajkowski, T. J. Walsh, T. A. Contreras, E. R. Schermer, and B. J. Carson (2015). Paleoseismic evidence for Late Holocene tectonic deformation along the Saddle Mountain fault zone, southeastern Olympic Peninsula, Washington, *Bull. Seismol. Soc. Am.* **105,** no. 1, 38–71, doi: 10.1785/0120140086.

Biasi, G. P., and R. J. Weldon (2006). Estimating surface rupture length and magnitude of paleoearthquakes from point measurements of rupture displacement, *Bull. Seismol. Soc. Am.* **96,** no. 5, 1612–1623, doi: 10.1785/0120040172.

Blakely, R. J., B. L. Sherrod, J. F. Hughes, M. L. Anderson, R. E. Wells, and C. S. Weaver (2009). Saddle Mountain fault deformation zone, Olympic Peninsula, Washington: Western boundary of the Seattle, *Geosphere* **5,** no. 2, 105–125, doi: 10.1130/GES00196.1.

Blakely, R. J., B. L. Sherrod, C. S. Weaver, R. E. Wells, A. C. Rohay, E. A. Barnett, and N. E. Knepprath (2011). Connecting the Yakima fold and thrust belt to active faults in the Puget Lowland, Washington, *J. Geophys. Res.* **116,** no. B07105, doi: 10.1029/2010JB008091.

Brocher, T. M., R. J. Blakely, and R. E. Wells (2004). Interpretation of the Seattle uplift, Washington, as a passive-roof duplex, *Bull. Seismol. Soc. Am.* **94,** no. 4, 1379–1401, doi: 10.1785/012003190.

Brocher, T. M., T. Parsons, R. J. Blakely, N. I. Christensen, M. A. Fisher, and R. E. Wells (2001). Upper crustal structure in Puget Lowland, Washington: Results from the 1998 seismic hazards investigation in Puget Sound, *J. Geophys. Res.* **106,** no. B7, 13,541–13,564, doi: 10.1029/2001JB000154.

Bucknam, R. C., E. Hemphill-Haley, and E. B. Leopold (1992). Abrupt uplift within the past 1700 years at southern Puget Sound, Washington, *Science* **258,** no. 5088, 1611–1614, doi: 10.1126/science.258.5088.1611.

Dragovich, J. D., and A. J. DeOme (2006). *Geologic Map of the McMurray 7.5-minute Quadrangle, Skagit and Snohomish Counties, Washington: With a Discussion of the Evidence for Holocene Activity on the Darrington-Devils Mountain Fault Zone*, Washington State Department of Natural Resources, Division of Geology and Earth Resources, Olympia, Washington.

Fialko, Y., D. Sandwell, M. Simons, and P. Rosen (2005). Three-dimensional deformation caused by the Bam, Iran, earthquake and the origin of shallow slip deficit, *Nature* **435,** no. 7040, 295–299, doi: 10.1038/nature03425.

Field, E. H., R. R. J. Arrowsmith, G. P. Biasi, P. Bird, T. E. Dawson, K. R. Felzer, D. D. Jackson, K. M. Johnson, T. H. Jordan, C. Madden, *et al.* (2014). Uniform California earthquake rupture forecast, version 3 (UCERF3)—The time-independent model, *Bull. Seismol. Soc. Am.* **104,** no. 3, 1122–1180, doi: 10.1785/0120130164.

Frankel, A., R. Chen, M. Petersen, M. Moschetti, and B. Sherrod (2015). 2014 update of the Pacific Northwest portion of the U.S. National seismic hazard maps, *Earthq. Spectra* **31,** no. S1, S131–S148, doi: 10.1193/111314EQS193M.

Frankel, A. D., M. D. Petersen, C. S. Mueller, K. M. Haller, R. L. Wheeler, E. V. Leyendecker, R. L. Wesson, S. C. Harmsen, C. H. Crramer, and D. M. Perkins (2002). Documentation for the 2002 update of the National Seismic Hazard Maps, *U.S. Geol. Surv. Open-File Rept. 02-420* 39 pp.

Hamling, I. J., S. Hreinsdóttir, K. Clark, J. Elliott, C. Liang, E. Fielding, E. Litchfield, P. Villamor, L. Wallace, T. Wright, *et al.* (2017). Complex multifault rupture during the 2016 M_w 7.8 Kaikōura earthquake, New Zealand, *Science* **356**, no. 6334, eaam7194, doi: 10.1126/science.aam7194.

Hemphill-Haley, M. A., and R. J. Weldon (1999). Estimating prehistoric earthquake magnitude from point measurements of surface rupture, *Bull. Seismol. Soc. Am.* **89,** no. 5, 1264–1279.

Johnson, S. Y., R. J. Blakely, W. J. Stephenson, S. V. Dadisman, and M. A. Fisher (2004). Active shortening of the Cascadia forearc and

implications for seismic hazards of the Puget Lowland, *Tectonics* **23,** no. 1, doi: 10.1029/2003TC001507.

Johnson, S. Y., S. V. Dadisman, D. C. Mosher, R. J. Blakely, and J. R. Childs (2001). Active tectonics of the Devils Mountain fault and related structures, northern Puget Lowland and eastern strait of Juan de Fuca region, Pacific Northwest, *U.S. Geol. Surv. Profess. Pap. 1643*, 45 pp., doi: 10.3133/pp1643.

Johnson, S. Y., A. R. Nelson, S. F. Personius, R. E. Wells, H. M. Kelsey, and B. L. Sherrod (2004). Evidence for late Holocene earthquakes on the Utsalady Point fault, northern Puget Lowland, Washington, *Bull. Seismol. Soc. Am.* **94,** no. 6, 2299–2316, doi: 10.1785/0120040050.

Kelsey, H. M., B. Sherrod, S. Y. Johnson, and S. V. Dadisman (2004). Land-level changes from a late Holocene earthquake in the northern Puget Lowland, Washington, *Geology* **32,** no. 6, 469–472, doi: 10.1130/G20361.1.

Kelsey, H. M., B. L. Sherrod, R. J. Blakely, and R. A. Haugerud (2012). Holocene faulting in the Bellingham forearc basin: Upper-plate deformation at the northern end of the Cascadia subduction zone, *J. Geophys. Res.* **117,** no. B3, doi: 10.1029/2011JB008816.

Kelsey, H. M., B. L. Sherrod, A. R. Nelson, and T. M. Brocher (2008). Earthquakes generated from bedding plane-parallel reverse faults above an active wedge thrust, Seattle fault, *Bull. Geol. Soc. Am.* **120,** nos. 11/12, 1581–1597, doi: 10.1130/B26282.1.

Mazzotti, S., H. Dragert, R. D. Hyndman, M. M. Miller, and J. A. Henton (2002). GPS deformation in a region of high crustal seismicity: N. Cascadia forearc, *Earth Planet. Sci. Lett.* **198,** no. 1, 41–48, doi: 10.1016/S0012-821X(02)00520-4.

McCaffrey, R., R. W. King, S. J. Payne, and M. Lancaster (2013). Active tectonics of northwestern U.S. inferred from GPS-derived surface velocities, *J. Geophys. Res.* **118**, no. 2, 709–723, doi: 10.1029/2012JB009473.

McKinney, W. (2010). Data structures for statistical computing in python, *Proc. of the 9th Python in Science Conf.*, Austin, Texas, Vol. 445, 51–56.

Meghraoui, M., H. Philip, F. Albarede, and A. Cisternas (1988). Trench investigations through the trace of the 1980 El Asnam thrust fault: Evidence for paleoseismicity, *Bull. Seismol. Soc. Am.* **78,** no. 2, 979–999.

Nelson, A. R., S. Y. Johnson, H. M. Kelsey, R. E. Wells, B. L. Sherrod, S. K. Pezzopane, L.-A. Bradley, R. D. Koehler, and R. C. Bucknam (2003). Late Holocene earthquakes on the Toe Jam Hill fault, Seattle fault zone, Bainbridge Island, Washington, *Bull. Geol. Soc. Am.* **115,** no. 11, 1388–1403, doi: 10.1130/B25262.1.

Nelson, A. R., S. F. Personius, J. Buck, L.-A. Bradley, R. E. Wells, and E. R. Schermer (2007). Field and laboratory data from an earthquake history study of scarps of the Lake Creek–Boundary Creek fault between the Elwha River and Siebert Creek, Clallam County, Washington, *U.S. Geol. Surv. Sci. Invest. Map 2961*, 2 sheets.

Nelson, A. R., S. F. Personius, B. L. Sherrod, H. M. Kelsey, S. Y. Johnson, L.-A. Bradley, and R. E. Wells (2014). Diverse rupture modes for surface-deforming upper plate earthquakes in the southern Puget Lowland of Washington State, *Geosphere* **10,** no. 4, 769–796, doi: 10.1130/GES00967.1.

Nelson, A. R., S. F. Personius, R. E. Wells, E. R. Schermer, L.-A. Bradley, J. Buck, and N. Reitman (2017). Holocene earthquakes of magnitude 7 during westward escape of the Olympic Mountains, *Bull. Seismol. Soc. Am.* **107,** no. 5, 2394–2415, doi: 10.1785/0120160323.

Oliphant, T. E. (2007). Python for scientific computing, *Comput. Sci. Eng.* **9,** no. 3, 10–20, doi: 10.1109/MCSE.2007.58.

Personius, S. F., R. W. Briggs, A. R. Nelson, E. R. Schermer, J. Z. Maharrey, B. L. Sherrod, S. A. Spaulding, and L.-A. Bradley (2014). Holocene earthquakes and right-lateral slip on the left-lateral Darrington–Devils Mountain fault zone, northern Puget Sound, Washington, *Geosphere* **10,** no. 6, 1482–1500, doi: 10.1130/GES01067.1.

Petersen, M. D., A. D. Frankel, S. C. Harmsen, C. S. Mueller, K. M. Haller, R. L. Wheeler, R. L. Wesson, Y. Zeng, O. S. Boyd, D. M. Perkins, *et al.* (2008). Documentation for the 2008 update of the United States National Seismic Hazard Maps, *U.S. Geol. Surv. Open-File Rept. 2008-1128*, 61 pp.

Porter, S. C., and T. W. Swanson (1998). Radiocarbon age constraints on rates of advance and retreat of the Puget Lobe of the Cordilleran ice sheet during the last Glaciation, *Quaternary Res.* **50,** no. 3, 205–213, doi: 10.1006/qres.1998.2004.

Pratt, T. L., K. G. Troost, J. K. Odum, and W. J. Stephenson (2015). Kinematics of shallow backthrusts in the Seattle fault zone, Washington State, *Geosphere* **11,** no. 6, 1948–1974, doi: 10.1130/GES01179.1.

Rockwell, T. K., and Y. Ben-Zion (2007). High localization of primary slip zones in large earthquakes from paleoseismic trenches: Observations and implications for earthquake physics, *J. Geophys. Res.* **112,** no. B10304, doi: 10.1029/2006JB004764.

Rosen, P. A., S. Hensley, I. R. Joughin, F. K. Li, S. N. Madsen, E. Rodriguez, and R. M. Goldstein (2000). Synthetic aperture radar interferometry, *Proc. IEEE* **88,** no. 3, 333–382.

Ryan, W. B. F., S. M. Carbotte, J. O. Coplan, S. O'Hara, A. Melkonian, R. Arko, R. A. Weissel, V. Ferrini, A. Goodwillie, F. Nitsche, *et al.* (2009). Global multi-resolution topography synthesis, *Geochem. Geophys. Geosys.* **10,** Q03014, doi: 10.1029/2008GC002332.

Schasse, H. W., and K. W. Wegmann (2000). *Geologic Map of the Carlsborg 7.5 Minute Quadrangle, Clallam County, Washington*, Washington Division of Geology and Earth Resources, Olympia, Washington.

Scott, D. W. (1992). *Multivariate Density Estimation*, John Wiley & Sons, New York, New York.

Sherrod, B. (2002). Late Quaternary surface rupture along the Seattle fault zone near Bellevue, Washington, *Eos Trans. AGU* **83,** F1074.

Sherrod, B., and J. Gomberg (2014). Crustal earthquake triggering by pre-historic great earthquakes on subduction zone thrusts, *J. Geophys. Res.* **119,** no. 2, 1273–1294, doi: 10.1002/2013JB010635.

Sherrod, B. L. (2001). Evidence for earthquake-induced subsidence about 1100 yr ago in coastal marshes of southern Puget Sound, Washington, *Bull. Geol. Soc. Am.* **113,** no. 10, 1299–1311, doi: 10.1130/0016-7606(2001)113<1299:EFEISA>2.0.CO;2.

Sherrod, B. L., E. Barnett, E. L. Schermer, H. M. Kelsey, J. Hughes, F. F. Foit, C. S. Weaver, R. Haugerud, and T. Hyatt (2013). Holocene tectonics and fault reactivation in the foothills of the north Cascade Mountains, Washington, *Geosphere* **9,** no. 4, 827–852, doi: 10.1130/GES00880.1.

Sherrod, B. L., R. J. Blakely, C. S. Weaver, H. M. Kelsey, E. Barnett, L. Liberty, K. L. Meagher, and K. Pape (2008). Finding concealed active faults: Extending the southern Whidbey Island fault across the Puget Lowland, Washington, *J. Geophys. Res.* **113,** no. B5, doi: 10.1029/2007JB005060.

Sherrod, B. L., T. M. Brocher, C. S. Weaver, R. C. Bucknam, R. J. Blakely, H. M. Kelsey, A. R. Nelson, and R. Haugerud (2004). Holocene fault scarps near Tacoma, Washington, USA, *Geology* **32,** no. 1, 9–12, doi: 10.1130/G19914.1.

Sherrod, B. L., R. C. Bucknam, and E. B. Leopold (2000). Holocene relative sea level changes along the Seattle fault at restoration Point, Washington, *Quaternary Res.* **54,** no. 3, 384–393, doi: 10.1006/qres.2000.2180.

Siedlecki, E. M., and E. Schermer (2007). Paleoseismology of the Boulder Creek fault, in *Geological Society of America Abstracts with Programs*, Vol. 39, Geological Society of America, Kendall, Washington, 26 pp.

Stirling, M., D. Rhoades, and K. Berryman (2002). Comparison of earthquake scaling relations derived from data of the instrumental and preinstrumental era, *Bull. Seismol. Soc. Am.* **92,** no. 2, 812–830, doi: 10.1785/0120000221.

ten Brink, U. S., P. C. Molzer, M. A. Fisher, R. J. Blakely, R. C. Bucknam, T. Parsons, R. S. Crosson, and K. C. Creager (2002). Subsurface geometry and evolution of the Seattle fault zone and the Seattle basin, Washington, *Bull. Seismol. Soc. Am.* **92,** no. 5, 1737–1753, doi: 10.1785/0120010229.

ten Brink, U. S., J. Song, and R. C. Bucknam (2006). Rupture models for the A.D. 900–930 Seattle fault earthquake from uplifted shorelines, *Geology* **34,** no. 7, 585–588, doi: 10.1130/G22173.1.

van der Walt, S., S. C. Colbert, and G. Varoquaux (2011). The NumPy array: A structure for efficient numerical computation, *Comput. Sci. Eng.* **13,** no. 2, 22–30, doi: 10.1109/MCSE.2011.37.

Van Wagoner, T. M., R. S. Crosson, K. C. Creager, G. Medema, L. Preston, N. P. Symons, and T. M. Brocher (2002). Crustal structure and relocated earthquakes in the Puget Lowland, Washington, from high-resolution seismic tomography, *J. Geophys. Res.* **107,** no. B12, 2381, doi: 10.1029/2001JB000710.

Vigny, C., A. Socquet, C. Rangin, N. Chamot-Rooke, M. Pubellier, M.-N. Bouin, G. Bertrand, and M. Becker (2003). Present-day crustal deformation around Sagaing fault, Myanmar, *J. Geophys. Res.* **108,** no. B11, 2533, doi: 10.1029/2002JB001999.

Walsh, T. J., and R. Logan (2007). Results of trenching the Canyon River fault, southeast Olympic Mountains, Washington, in *Geological Society of America Abstracts with Programs*,Vol. 39, Geological Society of America, 22–24.

Wang, E. (1997). Displacement and timing along the northern strand of the Altyn Tagh fault zone, northern Tibet, *Earth Planet. Sci. Lett.* **150,** nos. 1/2, 55–64.

Wells, D. L., and K. J. Coppersmith (1994). New empirical relationships among magnitude, rupture length, rupture width, rupture area, and surface displacement, *Bull. Seismol. Soc. Am.* **84,** no. 4, 974–1002.

Wells, R. E., C. S. Weaver, and R. J. Blakely (1998). Fore-arc migration in Cascadia and its neotectonic significance, *Geology* **26,** no. 8, 759–762.

Wesnousky, S. G. (2008). Displacement and geometrical characteristics of earthquake surface ruptures: Issues and implications for seismic-hazard analysis and the process of earthquake rupture, *Bull. Seismol. Soc. Am.* **98,** no. 4, 1609–1632, doi: 10.1785/0120070111.

Wilson, J. R., M. J. Bartholomew, and R. J. Carson (1979). Late Quaternary faults and their relationship to tectonism in the Olympic Peninsula, Washington, *Geology* **7,** no. 5, 235–239.

Witter, R. C., R. W. Givler, and R. J. Carson (2008). Two post-Glacial earthquakes on the Saddle Mountain West fault, southeastern Olympic Peninsula, Washington, *Bull. Seismol. Soc. Am.* **98,** no. 6, 2894–2917, doi: 10.1785/0120080127.

Zhang, G., C. Qu, X. Shan, X. Song, G. Zhang, C. Wang, J.-C. Hu, and R. Wang (2011). Slip distribution of the 2008 Wenchuan M_s 7.9 earthquake by joint inversion from GPS and InSAR measurements: A resolution test study: Slip distribution of 2008 Wenchuan earthquake, *Geophys. J. Int.* **186,** no. 1, 207–220, doi: 10.1111/j.1365-246X.2011.05039.x.

Manuscript received 28 May 2020
Published online 15 December 2020